

Membrane Tension–Mediated Growth of Liposomes

Siddharth Deshpande, Sreekar Wunnava, David Hueting, and Cees Dekker*

Recent years have seen a tremendous interest in the bottom-up reconstitution of minimal biomolecular systems, with the ultimate aim of creating an autonomous synthetic cell. One of the universal features of living systems is cell growth, where the cell membrane expands through the incorporation of newly synthesized lipid molecules. Here, the gradual tension-mediated growth of cell-sized ($\approx 10\ \mu\text{m}$) giant unilamellar vesicles (GUVs) is demonstrated, to which nanometer-sized ($\approx 30\ \text{nm}$) small unilamellar vesicles (SUVs) are provided, that act as a lipid source. By putting tension on the GUV membranes through a transmembrane osmotic pressure, SUV–GUV fusion events are promoted and substantial growth of the GUV is caused, even up to doubling its volume. Thus, experimental evidence is provided that membrane tension alone is sufficient to bring about membrane fusion and growth is demonstrated for both pure phospholipid liposomes and for hybrid vesicles with a mixture of phospholipids and fatty acids. The results show that growth of liposomes can be realized in a protein-free minimal system, which may find useful applications in achieving autonomous synthetic cells that are capable of undergoing a continuous growth–division cycle.

that of membranous containers such as liposomes, has so far been difficult to achieve and merits more attention and study.^[11]

In the life cycle of living cells, the mother cell undergoes a growth phase where it increases in mass by sequestering nutrients, synthesizing proteins, and replicating the genetic material which is eventually distributed to the daughter cells. To keep up with the increasing cell mass, the mother cell needs to increase its surface area to accommodate the volume increase. The increase in surface area is achieved by the tightly regulated synthesis and incorporation of lipids into the existing plasma membrane through a series of soluble and membrane-bound proteins as well as via vesicular trafficking and membrane fusion.^[12–15] Membrane fusion is in fact a ubiquitous biological process that plays a crucial role in diverse biological events such as cell-to-cell fusion (e.g., fertiliza-


1. Introduction

The staggering complexity of cells calls for in vitro approaches where one builds minimal biomolecular systems from the bottom up, to mimic and understand basic characteristics of life. Recently, there has been a rising trend toward reconstituting minimal biomolecular systems with purified biomolecules inside cell-like containers to generate self-sustaining, out-of-equilibrium systems and eventually design an autonomous synthetic minimal cell.^[1–5] Attempts to build such artificial cells will potentially help us understand the functioning of existing living systems as well as the origin of life, create new functional biomimetic structures, and design better therapeutics. Various crucial processes such as DNA replication, protein synthesis, cell morphogenesis and division, and rudimentary metabolic schemes are being actively studied in biomimicking containers.^[6–10] Dynamic growth is a prerequisite for the self-replication and eventual perpetuation of these synthetic microcompartments. Controlled growth, especially

tion, carcinogenesis), some pathways for viral entry into the cell, and intracellular processes (e.g., exocytosis, protein trafficking, vesicular transport).^[16,17] In cells, membrane fusion is mediated by highly specialized protein complexes such as soluble *N*-ethylmaleimide-sensitive factor attachment protein receptors (SNAREs) (for vesicle trafficking) and hemagglutinin (for viral invasions).^[18] These proteins are thought to function by accumulating local curvature stress and thus overcome the significant energy barrier for initiating the fusion process. The late stages of the fusion, which require large-scale membrane rearrangements, are also hypothesized to be driven by global physical factors such as the lateral membrane tension.^[19] Indeed, increased membrane tension was recently shown to increase the SNARE-mediated fusion efficiency.^[20] The potential of osmotic stress as a fusogen is also well-supported by the work on protein-free lipid systems^[19,21–23] and has been shown to enhance Ca^{2+} -mediated fusion processes.^[24] Molecular dynamics (MD) simulations have clearly shown that membrane tension alone can lead to pore opening by overcoming a characteristic energy barrier.^[25,26] Experimental work so far has mainly focused on studying bilayer and small unilamellar vesicles (SUVs) systems to provide evidence for the role of membrane tension on fusion processes.

Liposomes, vesicles where a phospholipid bilayer separates an aqueous inner volume from the outer aqueous environment, serve as good model systems for cells and are frequently employed for the bottom-up reconstitution of a minimal cell.^[27] Alternatively, fatty acid vesicles are studied as a model system for protocells that are hypothesized to have been involved in the emergence of life on the early earth. Bridging the gap

Dr. S. Deshpande, S. Wunnava, D. Hueting, Prof. C. Dekker
Department of Bionanoscience
Kavli Institute of Nanoscience Delft
Delft University of Technology
Van der Maasweg 9, 2629 HZ Delft, The Netherlands
E-mail: c.dekker@tudelft.nl

 The ORCID identification number(s) for the author(s) of this article can be found under <https://doi.org/10.1002/smll.201902898>.

DOI: 10.1002/smll.201902898

between the protocells and the modern cells, hybrid vesicles, which are composed of both lipids and fatty acids, have been studied as yet another model system.^[28] These hybrid systems are also potentially interesting scaffolds for synthetic cells as they exhibit a valuable combination of features, in particular an enhanced stability against Mg^{2+} , while retaining permeability to small charged molecules.^[28] Fatty acid and hybrid vesicles, when incubated with fatty acid micelles, grow by fusion of micelles with the vesicle.^[29–31] Phospholipid vesicles, when incubated in a bath of fatty acids, or when a fatty acid synthesis machinery is encapsulated within them, are also able to grow by the incorporation of free fatty acid molecules into the bilayer.^[32,33] But this approach is nonideal for establishing a continuous artificial cell cycle since it changes the lipid composition and the membrane properties of the vesicle. Attempts are being made to incorporate the lipid synthesis machinery within liposomes in order to achieve controlled growth of synthetic cells^[34–37] or reconstituting the genetic pathway for lipid synthesis using a cell-free expression system, albeit without realizing significant growth so far.^[38] The challenge has also been approached by using synthetic amphiphiles and phospholipid analogues, as well as by using autocatalytic reactions to continuously drive membrane synthesis.^[39–41] These various attempts at growing vesicles have shown good promise, but the final aim has not been achieved as of yet and highlight the challenging nature of membrane growth,^[11] especially for pure liposomes.

An alternative approach to achieve membrane growth is incorporation of preexisting lipid molecules or fusion with other vesicles.^[2] The critical micellar concentration of typical double-chain lipids is very low (in the nanomolar range^[42]), and they are virtually nonexchangeable with the surroundings once embedded within a membranous structure. Thus, it is highly impractical to grow the membrane efficiently by incorporating individual lipid molecules. Fusion with other amphiphilic assemblies (vesicles, micelles, etc.) appears to be a much more feasible option. Growth will then occur stepwise, with a step size that will strongly depend on the size of the “feeder assemblies.” Fusing, for example, many SUVs (<100 nm in diameter) to a mother giant unilamellar vesicle (GUV, $\approx 10\ \mu\text{m}$ in diameter) may exhibit growth that would proceed in a virtually continuous fashion, due to the very small increments involved. Till date, however, no attempts were reported to grow synthetic cells in this manner, i.e., to establish the controlled growth of GUVs exclusively by fusion with many SUVs.

In this paper, we use membrane tension as the principal control parameter to realize growth of GUVs by fusing many SUVs to them. For this approach, we produced hybrid vesicles, made up of lipids and fatty acids, as well as pure lipid vesicles, using a high-throughput on-chip microfluidic technique, octanol-assisted liposome assembly (OLA)^[43] that allows to sample large vesicle populations (>1000). Using this setup, we show that it is possible to induce vesicle growth via multiple fusion events with SUVs. We estimate that a significant fraction of the population ($\approx 20\%$) exhibited growth, of which a small fraction ($\approx 2\%$) was shown to even double its volume. We immobilized individual liposomes in microfluidic traps in order to track them over hours, yielding direct evidence of liposomes that clearly grew in size over time. A fluorescence-based membrane fusion assay (Eu-SDIP assay) showed that the observed

growth indeed resulted from SUV–GUV fusion events. Since the membrane compositions of mother and feeder vesicles are the same, this growth module can be potentially coupled with a division module^[44] to establish a continuous growth–division cycle of vesicles. Hence, the protein-free minimal growth technique that we present here has the potential to be used as one of the basic elements that will facilitate the quest toward developing autonomous synthetic cells.

2. Results

2.1. On-Chip Experimental Setup to Induce Liposome Growth

We set out to induce growth of mother GUVs by increasing their membrane tension to facilitate the subsequent fusion of feeder SUVs of the same membrane composition to the GUVs (Figure 1a). We produced GUVs ($\approx 10\ \mu\text{m}$ in diameter) using OLA.^[43] For observing a clean batch of GUVs, we modified the previously reported method to separate the liposomes from the waste product (1-octanol droplets),^[45,46] while still using density differences as the basis of separation: First, we punched a large collection well (4 mm in diameter) at the end of the production channel in order to collect GUVs at its bottom and let the waste product (1-octanol droplets) float to the top of the fluid-filled well. Next, we encapsulated dextran (molecular weight (M_w) = 6000) inside the GUVs that served a dual purpose: i) It induced sedimentation of the GUVs at the bottom of the well by making them denser than the environment (Figure 1b); ii) It acted as an osmolyte to induce the necessary membrane tension. Along with a population-level analysis which allowed us to obtain data from large population sizes ($n > 1000$), we also tracked individual GUVs using a previously published separation device,^[45] with an additional array of physical traps after the separation module, in order to immobilize purified GUVs.

We performed wide-field epifluorescence microscopy to observe the vesicles and obtain GUV images in the postjunction channel. For visualization, the vesicle membrane was doped with a small fraction of fluorescent lipids (0.1 mol% of 1,2-dioleoyl-*sn*-glycero-3-phosphoethanolamine-*N*-(lissamine rhodamine B sulfonyl), abbreviated as Rh-PE). Subsequently, the GUVs entered the collection well filled with an SUV-containing solution and settled to the bottom of the well. The SUVs, comprised of the same lipid composition, were prepared by extrusion (see the Experimental Section), and also contained a small fraction of fluorescent lipids (0.1 mol% of 1,2-dioleoyl-*sn*-glycero-3-phosphoethanolamine-*N*-(carboxyfluorescein) ammonium salt, abbreviated as PE-CF). End images were typically obtained after overnight incubation (>15 h) to ensure sufficient contact time with the SUVs. GUV diameters before and after the incubation were measured to obtain the respective size distributions and to evaluate vesicle growth (see the Experimental Section). If the GUVs were partially squeezed in the channel due to their diameter being larger than the channel height, the diameters were corrected to approximate spherical diameters, as described in Note S1 in the Supporting Information.

We hypothesized the fusion-induced GUV growth to work as follows. A liposome placed in a hypotonic solution develops a stressed membrane due to the influx of water as a result of the

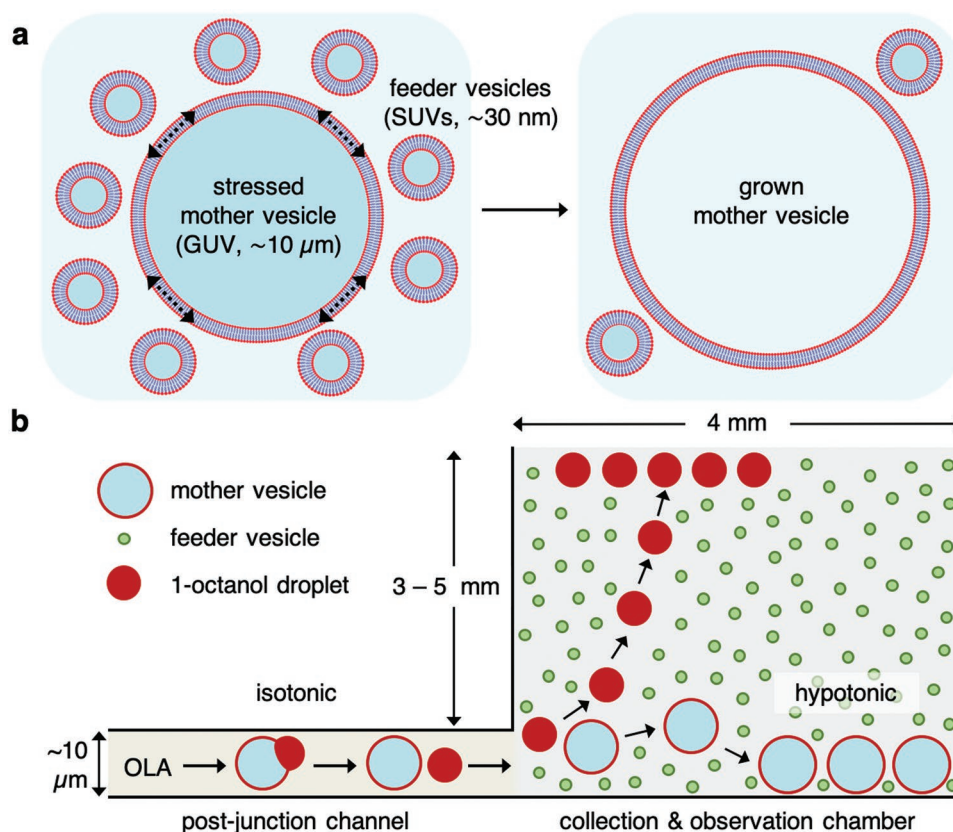


Figure 1. Concept and the experimental setup to attain membrane tension–mediated growth of GUVs. a) A stressed cell-sized ($\approx 10\ \mu\text{m}$) mother vesicle placed in a bath of nanometer-sized feeder vesicles ($\approx 30\ \text{nm}$) has the potential to fuse with them in order to relieve the membrane tension. This will cause the mother vesicle to grow until it is no longer stressed. b) Side-view schematic (not to scale) of the experimental setup. GUVs are produced using OLA, an on-chip microfluidic system, under isotonic conditions. The GUVs subsequently enter and settle to the bottom of a collection chamber, while 1-octanol droplets, a waste product, float to the top. The collection chamber is filled with a hypotonic solution containing feeder vesicles, stressing the membrane of mother vesicles and promoting fusion with the feeder vesicles.

applied osmotic pressure difference, $\Delta P_{\text{osm}} = \Delta cRT$. Here Δc is the concentration difference ($c_{\text{in}} - c_{\text{out}}$) across the membrane, R is the gas constant, and T is temperature. This influx of water is countered by the Laplace pressure, $P_{\text{Lap}} = 2\gamma/r$, where γ is the interfacial tension of the liposome and r is the liposome radius. At equilibrium, the osmotic pressure and the Laplace pressure cancel each other, yielding the interfacial tension on the membrane, $\gamma = \Delta cRT/2$. The critical membrane tension, above which the membrane disrupts, varies over a fairly wide range depending on the membrane composition ($3\text{--}30\ \text{mN m}^{-1}$), and it is about $10\ \text{mN m}^{-1}$ for a pure 1,2-dioleoyl-*sn*-glycero-3-phosphocholine (DOPC) membrane.^[47–49] This indicates that an initial Δc cannot be more than a few millimolar ($<5 \times 10^{-3}\ \text{M}$), for a GUV with a typical diameter of $10\ \mu\text{m}$. We kept the value of Δc between 2×10^{-3} and $4 \times 10^{-3}\ \text{M}$, with the intention to not disrupt the GUV but put its membrane under substantial tension to potentially drive the SUV–GUV fusion process. With every fusion, a finite amount of SUV membrane is incorporated into the GUV membrane, and the inner content of the SUV gets added to the GUV volume. As the SUVs have a larger surface-to-volume ratio, the GUV gains more surface area as compared to the volume. However, since the GUV is under hypotonic stress, the excess membrane re-stretches due to the finite influx

of water. This influx of water, in turn, dilutes the inner contents, slightly decreasing the osmolyte concentration. Thus, at every fusion, ΔP_{osm} and γ is relieved by a small amount, which sets a limit on the maximum number of fusions after which the GUV become isotonic. We further speculated that along with Δc , a high ratio of the two concentrations, $c_{\text{in}}/c_{\text{out}}$, would also be beneficial, in order to maintain the osmotic stress for a large number of fusions and prevent rapid dilution of the inner contents. Below we report experiments that test this scenario.

2.2. Tension-Mediated Growth of Hybrid Phospholipid/Fatty Acid Vesicles

We probed the growth potential of hybrid vesicles that were composed of equimolar amounts of phospholipids (DOPC) and fatty acids (oleic acid). The hybrid GUVs were formed under isotonic conditions. **Figure 2a** shows a snapshot of GUVs of similar sizes flowing in the postjunction channel, along with some bright 1-octanol droplets. The GUVs subsequently entered the SUV-containing collection well and experienced hypotonic conditions ($\Delta c = 2.4 \times 10^{-3}\ \text{M}$), thus experiencing a substantially increased membrane tension (an estimated

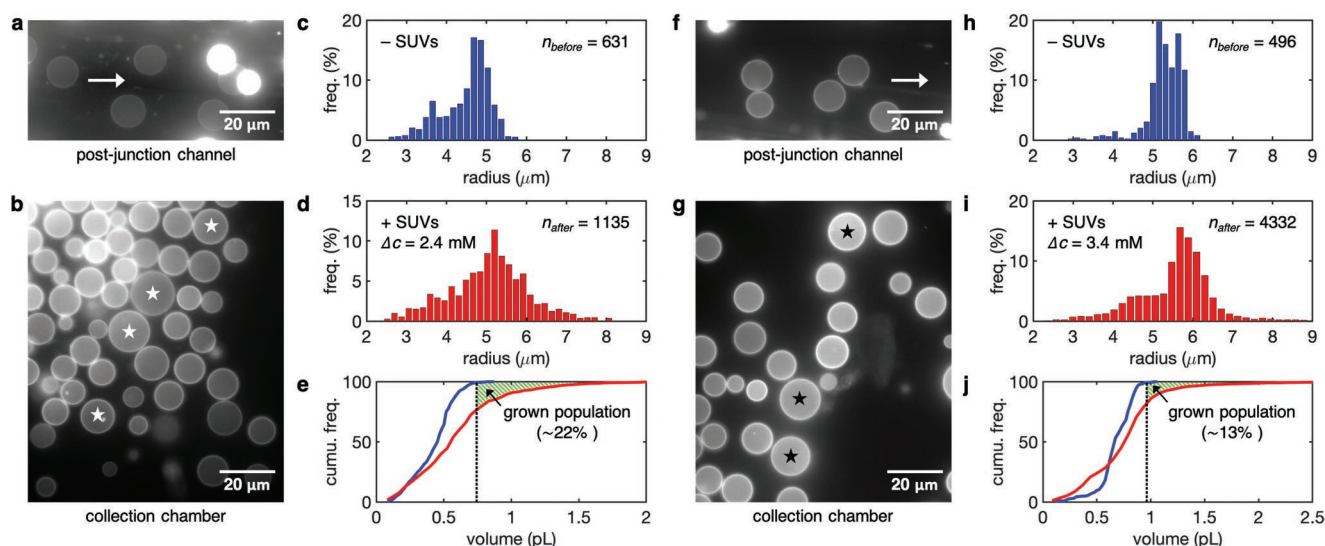


Figure 2. Membrane tension-mediated growth of hybrid (lipids/fatty acids) vesicles. Two separate experiments (a–e and f–j) showing an appreciable fraction of the hybrid vesicle population undergoing growth. a,f) Fluorescence images visualizing the vesicle membrane and representing the initial uniform size distribution of the vesicles in the postjunction channel. 1-octanol droplets can be seen as very bright objects. Arrows indicate the direction of flow. b,g) Typical field of views in the collection chamber showing a heterogeneous GUV size distribution with a few clear examples of grown vesicles that are marked by stars. c,h) Size distributions of GUVs before they enter the collection chamber. Note the absence of any big vesicles ($>6 \mu\text{m}$) in either of the distributions. d,i) Size distributions of GUVs present in the collection chamber, after incubation with SUVs under hypotonic conditions (d: $\Delta c = 2.4 \times 10^{-3}$ M, i: $\Delta c = 3.4 \times 10^{-3}$ M). Note the extended right tail of the distributions, indicating the presence of bigger vesicles ($6\text{--}8 \mu\text{m}$). e,j) Cumulative frequency percentage distributions of the GUV volumes before (blue curve) and after (red curve) experiencing stress-induced SUV fusion events, allowing the estimation of the minimal fraction of GUVs experiencing growth. Vertical dashed lines indicate the volumes below which 99% of the initial populations lie. This analysis indicated that at least 22% e) and 13% j) of the population grew to a vesicle size larger than the initial maximum, at lower and higher membrane tension, respectively.

average $\gamma \approx 13 \text{ mN m}^{-1}$). Figure 2b shows a typical field of view in the collection chamber after an overnight incubation with SUVs, showing a heterogeneous size distribution including a few clearly grown GUVs (indicated by stars). Figure 2c shows a relatively uniform initial size distribution with a mean radius of $4.5 \pm 0.6 \mu\text{m}$ ($n = 631$, coefficient of variation, $\text{CV} = 14\%$). The size distribution of vesicles after overnight incubation can be seen in Figure 2d. As can be observed, the final distribution became broader and was shifted to the right, giving a mean final radius $5.1 \pm 1.0 \mu\text{m}$ ($n = 1135$, $\text{CV} = 19\%$). Notably, the maximum value observed in the initial distribution was $5.8 \mu\text{m}$, but $8.2 \mu\text{m}$ in the final distribution. The presence of much larger GUVs as compared to the initial ones clearly indicated that a certain fraction of the GUV population grew, presumably by undergoing multiple fusion events with the SUVs in the surrounding solution. To corroborate that the observed growth was driven by the membrane fusion with SUVs, we carried out control experiments in the absence of SUVs, but still in a hypotonic bath, so as to apply the same level of osmotic stress ($\Delta c = 2.8 \times 10^{-3}$ M, $\gamma \approx 19 \text{ mN m}^{-1}$). Here, we found that the initial and the final distributions were quite identical, and no large liposomes were observed, as can be observed in Figure S1 in the Supporting Information. The cumulative frequency distribution indicated that in both the cases, 99% of GUVs were under 1.4 pL , consistent with the absence of any significant growth. Furthermore, we can rule out that fatty acids themselves mediate or trigger growth without the need of membrane tension, as previous studies have clearly shown that

hybrid vesicles are able to grow only in presence of pure fatty acid vesicles, and not in presence of hybrid vesicles.^[31] This observation is further strengthened by a recent study, where the surface area of hybrid vesicles with 50% or higher phospholipid content was shown to remain completely constant in presence of Mg^{2+} , proving the ability of phospholipids to efficiently retain the fatty acids in the hybrid membranes.^[28]

To estimate the fraction of the population of GUV that exhibited growth, we plotted the cumulative percentage frequency distribution of the vesicle volumes (Figure 2e). These distributions show that 99% of the mother GUVs had an initial volume smaller than 0.7 pL (blue curve), a number that dropped to 77% of liposomes after incubation with SUVs (red curve), suggesting that at least 22% of liposomes underwent growth to variable extents. Note that the maximum possible swelling ($\approx 5\%$ increase in the surface area^[50,51]) of the GUVs after experiencing a hypotonic solution was already taken into consideration in calculating the growth. The value of 22% is in fact an underestimation, as it disregards any small liposomes that might have grown but were still not bigger than the largest liposomes in the initial distribution. Furthermore, we estimated the minimum population fraction that doubled its volume, yielding an (under)estimate of 2.1% of the vesicle population that was achieving a minimum 100% increase in volume.

We then conducted a similar experiment, but with a higher concentration difference ($\Delta c = 3.4 \times 10^{-3}$ M), to see if an increased membrane tension would lead to an increased growth. Figure 2f,g show images of the initial GUVs and of

GUVs after incubation with SUVs, respectively. Again a heterogeneous size distribution was observed with a number of clearly grown GUVs (indicated by stars). More data are shown in Figure S2 in the Supporting Information. The initial monodisperse size distribution of the GUVs, with a mean radius of $5.3 \pm 0.5 \mu\text{m}$ and a CV = 9% ($n = 496$, Figure 2h), was subjected to a considerably higher average membrane tension ($\gamma \approx 22 \text{ mN m}^{-1}$). The final size distribution had an increased mean radius of $5.6 \pm 0.9 \mu\text{m}$ and a larger CV = 16% ($n = 4332$), with a maximum value of $9.5 \mu\text{m}$ as compared to the $6.2 \mu\text{m}$ value seen in the initial distribution (Figure 2i). The cumulative percentage frequency distribution indicated that at least 13% of the population underwent significant growth (Figure 2j). The data also indicate that a minimum of 1.6% of the population at least doubled in its volume. We thus find, contrary to our expectations, that a membrane tension closer to the lysis tension did not improve, but rather worsened the efficiency of growth. A likely reason for this is that vesicles are much more prone to bursting at such high tensions, leading to burst-and-reseal events that help lower the tension—see below also. In fact, the left shoulder in the final distribution strongly supports this.

2.3. Tension-Mediated Growth of Phospholipid Liposomes

After successfully growing hybrid vesicles, we investigated the possibility to grow phospholipid vesicles, without any fatty acids. We chose for a mixture of DOPC, 1,2-dioleoyl-*sn*-glycero-3-phosphoethanolamine (DOPE), and 1-hydroxy-2-oleoyl-*sn*-glycero-3-phosphocholine (LPC) in a molar ratio of 70:15:15. DOPE was added because of its fusogenic nature, due to its inverted cone shape that leads to increased membrane curvature.^[52] While a binary mixture of just DOPC and DOPE (see the next section) can also be used, we observed that the liposome production, specifically the time required for the 1-octanol pocket to separate, was adversely affected by the presence of DOPE. We speculated that the inverted cone-shaped DOPE (having a negative spontaneous curvature) might be stabilizing the pocket-bilayer interface and could perhaps be compensated by the addition of cone-shaped (having a positive spontaneous curvature) LPC lipids. Indeed, we observed the desired effect and a much faster pocket separation in presence of LPC. The initial size distribution of the liposomes in postproduction channel ($n = 666$) is given in Figure 3a. Upon applying $\Delta c = 2.6 \times 10^{-3} \text{ M}$ (corresponding to $\gamma \approx 11 \text{ mN m}^{-1}$; $n = 769$) and incubation with the SUVs, the evolved distribution, shown in Figure 3b, showed an extended right tail. This indicated the presence of bigger liposomes, with the maximum value of $6.0 \mu\text{m}$ as compared to $3.8 \mu\text{m}$ for the initial distribution. A cumulative percentage distribution of the radii indicated that at least 14% of the population experienced growth, as only 86% of the population was below 0.2 pL , compared to 99% as observed for the initial population. It also indicated that at least 2% of the population did double in volume.

To prove that the observed growth is due to the SUVs fusing with the liposomes, a fluorescence-based fusion assay was performed. EuCl_3 was encapsulated within the SUVs, while SDIP, a complexing ligand for Eu^{3+} , was encapsulated inside the liposomes. Both components are not fluorescent on their

own but upon SUV–GUV fusion, the released Eu^{3+} will form a fluorescent complex with SDIP. An exemplary liposome flowing in the production channel before encountering the SUVs, and showing a negligible fluorescence in its lumen, is shown in Figure 3d. However, upon encountering the SUV-containing hypotonic ($\Delta c = 3.3 \times 10^{-3} \text{ M}$) solution in the collection well, some liposomes started to show an increased fluorescence in their lumen (Figure 3e), providing firm evidence that the SUVs fused with the GUVs. Figure 3f compares these two fluorescence intensity distributions, before and after encountering the SUVs, showing a definite fraction of higher intensity for liposomes incubated with SUVs. A double Gaussian fit to the distribution indicated a mean fluorescence value of 79 for the first peak and a mean value of 143 for the second peak, i.e., close to twice higher fluorescence intensity. The majority of the liposomes showed no significant increase in the fluorescence value, which corresponds well with the fact that we only see a finite fraction of the entire population undergoing growth. To sum up, the fusion assay successfully demonstrated that the SUVs mixed their contents with that of the GUVs and thus underwent a complete fusion process, as opposed to, for example, stalling at a hemifusion state.

We also examined the possibility to attain growth from the internal environment, by encapsulating the SUVs inside the mother liposomes. The SUVs were thus added in the inner aqueous solution while, similar to the previous experiments, an osmotic stress was induced once the liposome entered the collection well ($\Delta c = 2.8 \times 10^{-3} \text{ M}$). The initial monodisperse size distribution (Figure 3g, mean radius $5.1 \pm 0.5 \mu\text{m}$, $n = 351$) clearly became wider after incubation in the hypotonic environment, especially exhibiting an extended right tail (Figure 3h, mean radius of $5.4 \pm 0.7 \mu\text{m}$, $n = 1153$), suggesting that a significant fraction of liposomes had grown. Initially, 99% of liposomes were below 0.8 pL whereas after incubation the percentage dropped to 76%, indicating that 23% of the liposome grew to variable extents. Thus, we conclude that we were able to grow liposomes substantially, independent of the localization of SUVs with respect to the GUVs, i.e., from the inside or outside of the liposome.

2.4. Observing Growth Events of Individual Vesicles in Microfluidic Traps

The population analyses allowed us to understand the general trends of tension-mediated growth of GUVs. However, this only quantized the initial and the final GUV population sizes, and did not yield information on the dynamics at the level of individual vesicles. In order to capture the growth process at a single-liposome level, we utilized a more sophisticated setup involving microfluidic traps. These physical traps were integrated into a design used for on-chip density-based separation of liposomes from 1-octanol droplets,^[45] right after the separation hole. A feeding channel was used to subsequently flow the SUV-containing solution along the traps. We used two different types of traps: i) We scaled down a previously reported design that was used for trapping larger objects^[53] (e.g., embryos) to match the $\approx 10 \mu\text{m}$ liposome dimensions. ii) We also used a straightforward design consisting of individual rectangular

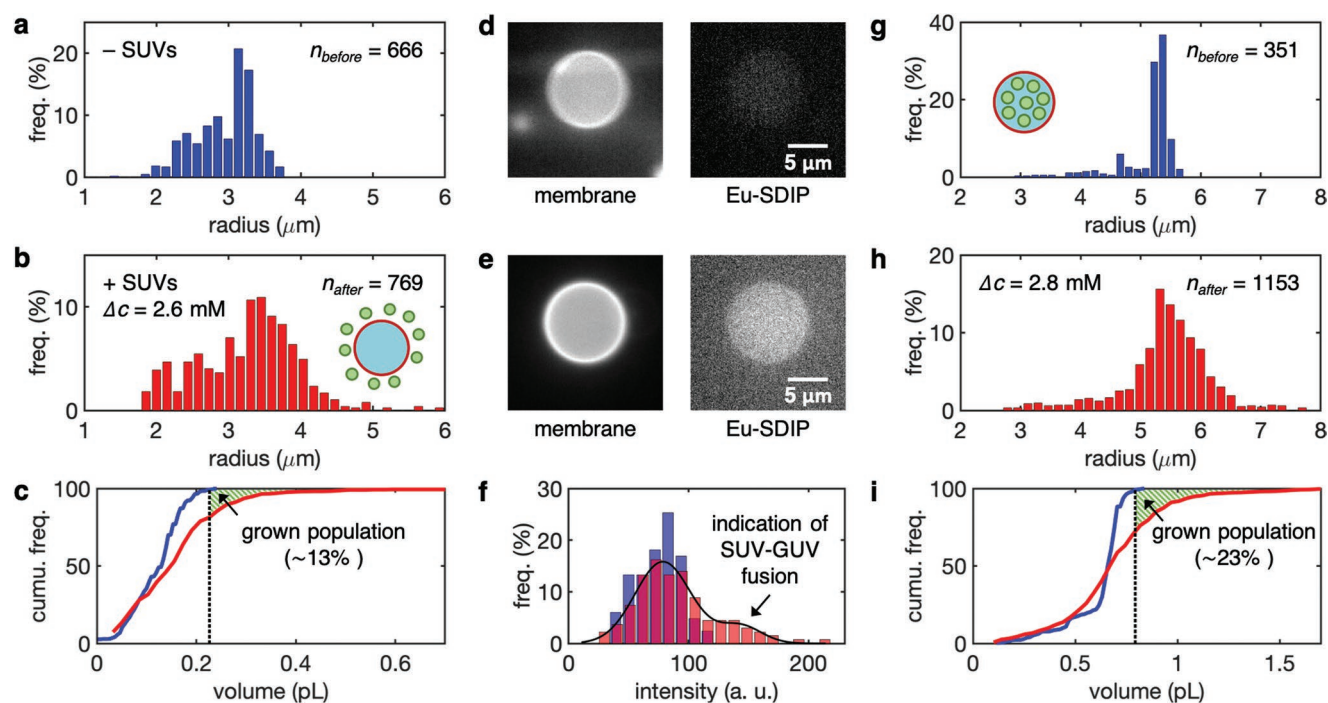


Figure 3. Membrane tension-mediated growth of liposomes. a) Initial size distribution of liposomes. Note the absence of any big vesicles ($>4 \mu\text{m}$). b) Final size distribution of liposomes, after incubation with SUVs under hypotonic conditions ($\Delta c = 2.6 \times 10^{-3} \text{ M}$). Note the extended right tail of the distribution, indicating the presence of bigger vesicles (4–6 μm). c) Cumulative frequency percentage distributions of the liposome volumes before (blue) and after (red) experiencing stress-induced SUV fusion events. Vertical dashed line indicates the volume below which 99% of the initial populations lie. The analysis (under)estimated that about 13% of the population grew. d) A fluorescence image of a typical liposome encapsulating SDIP in the production channel, before encountering SUVs. e) A fluorescence image of a liposome placed in a hypotonic SUV-containing solution, showing fluorescence arising from the Eu-SDIP complex, thus pointing toward SUV–GUV fusion events and mixing of their internal contents. f) Fluorescence intensity distributions of the liposomal lumen, in the postjunction channel (blue histogram) and in the collection well, 1.5 h after incubation with SUVs (red histogram). While the majority of the latter distribution overlaps with the former one, a second smaller peak indicates the population that was subjected to multiple fusion events. The black curve is a double Gaussian fit. g) Initial size distribution of liposomes encapsulating SUVs. Note the absence of any big vesicles ($>6 \mu\text{m}$). h) Final size distribution of liposomes under hypotonic conditions ($\Delta c = 2.8 \times 10^{-3} \text{ M}$). Note the extended right tail of the distribution, indicating the presence of bigger vesicles (6–8 μm). i) Cumulative frequency percentage distributions of the liposome volumes before (blue) and after (red) experiencing stress-induced SUV fusion events. Vertical dashed line indicates the volume below which 99% of the initial populations lie. The analysis (under)estimated that about 23% of the population grew.

traps. Images of arrays of these on-chip traps are shown in Figure S3 in the Supporting Information. While the traps were efficient in capturing the liposomes, their presence increased the hydraulic resistance of the postseparation hole channel, adversely affecting the separation of 1-octanol droplets from the liposomes. Nevertheless, we managed to trap a sufficient number of liposomes, allowing to observe individual liposomes over hours, and to obtain convincing evidence for growth at a single liposome level.

We captured movies of liposomes, composed of DOPC and DOPE in the molar ratio 7:3, that showed clear signatures of growth, i.e., they increased in their diameter over the course of hours. We did not use LPC in this case, showing that LPC simply aided the pocket separation process and was not necessary to bring about liposome growth. For these experiments, we used polyethylene glycol (PEG) as the osmolyte and we used two different concentration differences ($\Delta c = 1.9 \times 10^{-3}$ and $3.8 \times 10^{-3} \text{ M}$) to examine the effect of a lower ($\approx 10 \text{ mN m}^{-1}$) and higher membrane tension ($\approx 18 \text{ mN m}^{-1}$) on growth. Figure 4a (also see Video S1 in the Supporting Information) shows a time-lapse of

a trapped liposome that steadily grew over the course of a few hours. Figure 4c shows the corresponding quantification of the event showing that the liposome increased its diameter by about 24% over the course of 5 h, which corresponds to a very significant (90%) increase in its volume. The growth rate was much higher at the beginning and plateaued over time. This is expected, because the membrane tension is relieved with every fusion until the stress is relieved to the point where fusion events are no longer promoted. Next to straightforward liposome growth, we observed two other types of events: pulsatile behavior (Figure 4b) and the absence of growth. In case of pulsatile behavior, the liposome exhibited a small increase in the diameter ($\approx 5\%$), before undergoing an abrupt change back to original diameter, indicating pore formation and resealing (Figure 4d,e). Such pulsing behavior is well documented and is known to happen in the case of osmotic pressure-induced membrane stress.^[51,54] Figure 4b (also see Video S2 in the Supporting Information) shows a typical example of a pulsating liposome, where the liposome repeatedly grew and shrunk before finally bursting and resealing into a much smaller liposome that remained stable

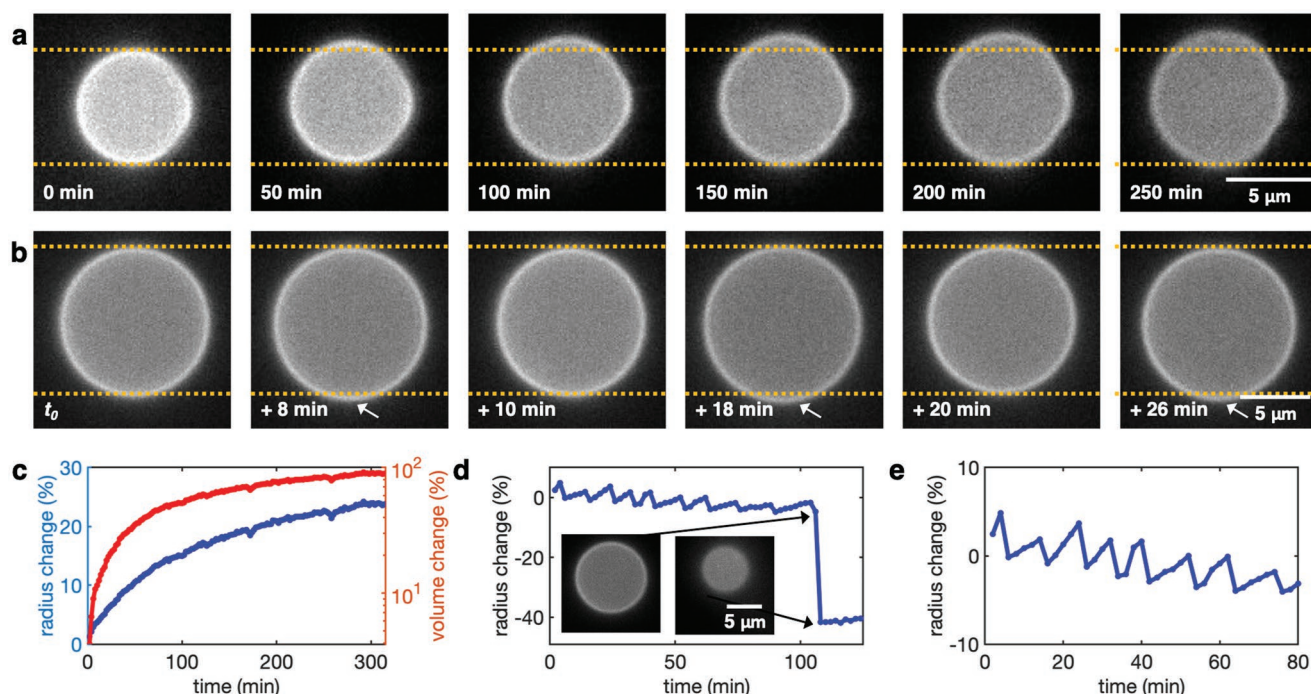


Figure 4. Individual liposomes confined within physical traps showing growth and pulsatile behavior under membrane stress. a) Time-lapse images visualizing the membrane of a growing liposome. The slight indentation observed in the liposome is due to the flow of the feeding solution pushing it into the trap. b) Time-lapse images visualizing the membrane of a pulsating liposome. A slight periodic increase in the liposome diameter is indicated with arrows. c) Percentage increase in the radius and volume of the liposome shown in (a), as a function of time. d) Percentage change in the radius of the liposome shown in (b), as a function of time. The liposome eventually undergoes a sudden collapse before resealing itself into a much smaller liposome (see insets). e) A zoom-in of the initial pulsing behavior, showing a radius change of up to 5% with each pulse. The dashed horizontal lines in a and b are drawn in order to guide the eye to see the change in the diameter.

in time (Figure 4d). Such events also explain the heterogeneous size distribution that we observed, described in the previous sections, in particular the presence of small liposomes comprising the left tail in distributions such as Figure 2a,i.

Both in case of lower and higher tension ($n = 20$ and 18, respectively), about 30% of the liposomes exhibited growth, with the average growth resulting in a $\approx 80\%$ increase in volume. While about half of the population showed pulsating behavior in both cases, the extent of pulsing, specifically the number of pulses observed, was much more pronounced when the interfacial tension was higher: At lower tension, the average number of pulses exhibited by liposomes was 3, which increased to 9 in case of higher tension. Furthermore, the mean radius of pulsating liposomes was $4.8 \pm 1.0 \mu\text{m}$ in case of lower tension and $4.2 \pm 0.8 \mu\text{m}$ in case of higher tension, indicating that the pulsing behavior was correlated with the increased membrane tension. About 17–25% of liposomes showed neither growth nor any pulsatile behavior, i.e., their diameter remained constant. It is possible that they underwent a pulsatile behavior or a rupture–reseal event before they were trapped, equilibrating the osmotic pressure and thus preventing any dynamic behavior. To confirm that the obtained growth was a result of membrane stress, we performed a negative control in presence of SUVs but with liposomes having no osmotic pressure difference across the membrane. As expected, we did not see any signs of growth in any of the trapped liposomes, over a similar time period (16 h, 1d,

Supporting Information). This simultaneously also eliminated the possibility that SUV fusion and hence GUV growth was induced by PEG, which is known to be able to promote fusion at high concentrations.^[55]

The obtained time-lapse data on individual liposomes in traps corresponded well with the results that we previously obtained at the population level. Nevertheless, it should be noted that slightly different lipid compositions were used for the two cases (with and without LPC), whose effect cannot be completely ruled out. Using the time-lapse monitoring of individual liposomes, we observed a variety of behaviors, viz., continuous growth, pulsatile behavior, or a stable nonvarying size, consistent with the pronouncedly heterogeneous size distribution of liposomes that settled in the collection chamber. The data suggest that the heterogeneity derives from the fact that GUVs under membrane stress are prone to membrane rupture as well as temporary pore formation and resealing. The growth potential of a particular liposome therefore depends on its history, i.e., whether it has suffered from any previous burst–reseal event and hence if the membrane is still under an optimal amount of stress.

3. Discussion

In this paper, we aimed at using membrane tension as the prevailing parameter to bring about the fusion of nanometer-sized

feeder vesicles to cell-sized mother vesicles, in order to grow them in a minimal fashion. Using a microfluidic setup, we successfully demonstrated the growth of osmotically stressed vesicles ($\approx 10\ \mu\text{m}$ in diameter) by fusing many unilamellar vesicles (30 nm in diameter) to them. Under hypotonic conditions, the increased membrane tension on the bilayer ($10\text{--}20\ \text{mN m}^{-1}$) led to fusion events between SUVs and the mother GUVs, allowing an appreciable fraction (15–25%) of the population to grow. We were able to grow hybrid (vesicles made up of fatty acids and phospholipids) as well as pure phospholipid vesicles, of different lipid compositions, in this fashion. We designed a simple and a minimal system, with as little interacting components as possible. In principle, as long as the key parameters (appropriate osmotic conditions, absence of fusion-interfering or fusion-promoting components) remain the same, we expect such growth assay to work in the same way also in presence of additional solutes and ionic buffers.

Our analysis indicated that a minor fraction was able to more than double its volume, sometimes even up to 300%. This volume increase corresponds to thousands of SUV fusion events, followed by water influx, as described in the Results Section. We attribute the observed heterogeneity to grow to the fact that under stress, vesicles can form transient pores in their membrane and release solutes lowering the osmotic pressure difference.^[51,54] This process may continue in an oscillatory manner till all the tension is relieved. Indeed, we very frequently observed such pulsating behavior when tracking individual liposomes. Because the membrane tension is directly proportional to the vesicle radius, it implies that, for a given Δc , larger GUVs are more stressed and more fusogenic as compared to the smaller ones, but they are also more prone to bursting. Thus, keeping a monodisperse vesicle population under just enough membrane tension (about $10\ \text{mN m}^{-1}$) should promote growth optimally while avoiding pore formation and lysis.

While the increased membrane tension, in principle, should also promote GUV-GUV fusion, we never observed such events. This may be due to many reasons: First, we observed a very heterogeneous growth, possibly because many GUVs released their membrane tension by equilibrating with the environment through formation of transient pores. This decreased the probability of two stressed GUVs coming into contact with each other. Furthermore, OLA requires poloxamer 188 (P188), a nonionic triblock copolymer surfactant, in the outer aqueous phase. P188 has a tendency to weakly adsorb on the membrane surface.^[56] While the exit/feeding solution did not contain P188, it is possible that some P188 remained adsorbed on the GUV membrane. The presence of P188 may have prevented GUV-GUV fusion, while still allowing 30 nm SUVs to fuse with the GUVs. Lastly, when the GUVs entered the well, they got dispersed in a large solution volume ($>10\ \mu\text{L}$) containing very high density of SUVs ($\approx 10^5$ liposomes/pL), immediately leading to potential fusion events with the SUVs. While the overnight incubation ultimately resulted in clustering of the GUVs at the bottom of the chamber due to some residual flow in the system, it is highly unlikely that the GUVs had the opportunity to come into sufficient contact with each other for the majority of the experiment duration.

In addition to dedicated membrane fusion proteins, a variety of fusogenic agents have been reported to promote membrane

fusion, such as divalent cations, electrostatic interactions, volume depletion, electric pulse, and synthetic constructs such as DNA–lipid conjugates.^[11,57–63] Here, we presented convincing experimental evidence that membrane tension alone is sufficient to induce membrane fusion, in the absence of any other fusogens. This provides strong support for the hypothesis that membrane stress is the root cause of membrane fusion, including those mediated through proteins.^[19] Simulations have indeed indicated that fusion is a prominent way for releasing the tension in the membrane and providing sufficient membrane tension ($\gamma = 50\ \text{mN m}^{-1}$) alone can drive fusion.^[25,64] We provided direct experimental evidence that the membrane stress alone can make the liposomes grow very substantially in size, even doubling their volume in some cases.

These GUVs can be potentially subjected to division, for example in a mechanical way,^[44] to ultimately establish an artificial cycle of vesicles.^[44] The protein-free approach presented in this work to achieve growth of stressed vesicles thus presents a step forward to develop artificial cells that are capable of showing living cell-like characteristics using minimal components.

4. Experimental Section

Materials and Solution Compositions: Polyvinyl alcohol (PVA; M_w 30000–70000; 87–90% hydrolyzed), glycerol, poloxamer 188 (P188), 1-octanol, NaOH, glucose, dextran (M_w 6000), PEG (M_w 8000), and oleic acid were purchased from Sigma-Aldrich. AF647-dextran (M_w 10000) was purchased from Thermo Fisher Scientific. SDIP and EuCl_3 for membrane fusion assay were purchased from Biotium. Lipids (DOPC, DOPE, LPC, Rh-PE, and PE-CF) and oleic acid were purchased from Avanti Polar Lipids. The inner aqueous compositions were as follows: 15% v/v glycerol, 1.8% w/v dextran, 0.004% w/v AF647-dextran (Figure 2a–e); 15% v/v glycerol, 2.4% w/v dextran, 0.004% w/v AF647-dextran (Figure 2f–j and Figure 3a–c; Figures S1a–c and S2, Supporting Information); 15% v/v glycerol, 1.8% w/v dextran, $1 \times 10^{-3}\ \text{M}$ SDIP (Figure 3d–f); 15% v/v glycerol, 2.4% w/v dextran, 0.004% w/v AF647-dextran, 1% w/v SUV solution (Figure 3g–i); 15% v/v glycerol, 3% w/v PEG, 0.004% w/v AF647-dextran (Figure 4a; Movie S1, Supporting Information); 15% v/v glycerol, 4% w/v PEG, 0.004% w/v AF647-dextran (Figure 4b; Figure S1d and Movie S2, Supporting Information). The lipids/fatty acids were dissolved in 1-octanol in order to have a final total concentration of 0.2% w/v. The specific compositions of lipids/fatty acids, in terms of molar ratios, were as follows: oleic acid: DOPC (1:1; Figure 2; Figures S1a–c and S2, Supporting Information); DOPC: DOPE: LPC (7:1.5:1.5; Figure 3); DOPC: DOPE (7:3; Figure 4; Figure S1d and Videos S1–S2, Supporting Information). A fluorescent lipid, Rh-PE, was present in all the solutions at 0.1 mol%. The stock solutions (10% w/v) were prepared in ethanol as described elsewhere,^[46] and appropriate amounts were dissolved in 1-octanol just before experimentation. The outer aqueous compositions were as follows: 15% v/v glycerol, $3 \times 10^{-3}\ \text{M}$ glucose, 5% w/v P188 (Figure 2a–e and Figure 3a–c); 15% v/v glycerol, $4 \times 10^{-3}\ \text{M}$ glucose, 5% w/v P188 (Figure 2f–j, Figure 3d–i, Figures S1a–c and S2, Supporting Information); 15% v/v glycerol, 3% w/v PEG, 5% w/v P188 (Figure 4a, Movie S1, Supporting Information); 15% v/v glycerol, 4% w/v PEG, 5% w/v P188 (Figure 4b; Movie S2, Supporting Information). The compositions of the exit/feeding solutions, i.e., the fluid dispensed in the collection well or flown over the trapped liposomes were as follows: 15% v/v glycerol, 0.2% w/v SUV solution (Figure 2 and Figure 3a–f; Figure S2, Supporting Information); 15% v/v glycerol, $1.3 \times 10^{-3}\ \text{M}$ glucose (Figure 3g–i; Figure S1a–c, Supporting Information); 15% v/v glycerol, 0.13% w/v SUV solution (Figure 4a; Video S1, Supporting Information); 15% v/v glycerol, 0.06% w/v SUV solution (Figure 4b; Figure S1d and Video S2, Supporting Information).

Liposome Production Using OLA: The detailed working of OLA and its troubleshooting is available in the online protocol.^[46] Briefly, the microfluidic channels were fabricated on a silicon wafer using e-beam lithography, followed by dry etching, and finally, surface silanization. The height of the patterned structures was measured using a stylus profiler DektakXT (Bruker Corporation) and was either 6.8 or 9.4 μm for the devices used in population-level experiments and either 8.4 or 9.4 μm for the devices used in single liposome-level experiments. Polydimethylsiloxane (PDMS)-based microfluidic devices were prepared and surface-treated as described elsewhere^[65] in case of experiments involving the collection chamber, or as described in the online protocol^[46] in case of experiments involving microfluidic traps. In the former case, 5% w/v PVA solution was used for surface treatment, while the concentration was reduced to 2.5% w/v in the latter case.

The microfluidic approach allowed to obtain data from large population sizes ($n \approx 1000$), albeit with an occasional compromise on the sample monodispersity due to two main reasons: i) Occasional modulation of pressures at the production junction in order to ensure continuous GUV production, which resulted in modest size variation. ii) Unwanted bursting-and-resealing of GUVs in the postjunction channel over prolonged production due to wearing-off of the surface treatment and presence of physical obstacles (e.g., dirt particles), giving rise to smaller GUVs.

Preparation of SUVs: SUVs were prepared by lipid film hydration, followed by extrusion. Appropriate amounts of lipid/fatty acid stock solutions in chloroform were taken in a round bottom flask. Chloroform was evaporated by blowing with a stream of nitrogen to obtain a thin film of lipids/fatty acids. Remaining traces of chloroform were removed by keeping the flask under partial vacuum for at least 2 h in a desiccator. The film was hydrated with a solution to a final lipid concentration of either 2% w/v (Figures 2,3; Figure S2, Supporting Information) or 0.25% w/v (Figure 4; Videos S1–S2 and Figure S1d, Supporting Information). If needed, the hydration was facilitated by incubating at 37 °C while shaking for at least 30 min till the entire film was dispersed in the solution. Optionally, the dispersed film was kept for 30 min in an ultrasonic bath in order to break large aggregates and thus ease the extrusion step. A minixtruder (Avanti Polar Lipids) was assembled and set on a heating block at 70 °C.^[66] The lipid suspension was passed through a 100 nm, and then through a 30 nm polycarbonate track-etched membrane (Whatman), 21 times each. While the extrusion step could have been carried out at room temperature, the viscosity of glycerol was substantially reduced (more than 2.6 times^[67]) at 70 °C, as compared to the value at room temperature (20 °C), thus facilitating the extrusion process. The small size of SUVs was chosen because the fusogenic potential increases with decrease in the vesicle size, due to the higher curvature.^[68] The extruded SUVs were then stored at 4 °C and used as fresh as possible, usually within a week. The compositions of the buffers used to prepare SUVs were as follows: 15% v/v glycerol, 3% w/v dextran, 10×10^{-3} M NaOH (Figure 2; Figure S2, Supporting Information); 15% v/v glycerol, 2.4% w/v dextran (Figure 3a–c and Figure 3g–i); 15% v/v glycerol, 1.8% w/v dextran, 1×10^{-3} M EuCl_3 (Figure 3d–f); 15% v/v glycerol, 3% w/v PEG (Figure 4a; Video S1, Supporting Information), 4% w/v PEG (Figure 4b; Figure S1d and Video S2, Supporting Information). Since extrusion is a bulk technique, the inner contents of the SUVs had the same composition as the surrounding buffer. The SUV lipid composition was kept exactly the same as the corresponding GUV lipid composition for each of the experiments. It should be noted that the concentration of the polymers (dextran, PEG) used in the experiments was much less than at which the nonideal osmotic behavior sets in, which happens at much higher concentrations (>10% w/v).^[69,70]

Image Acquisition and Analyses: An Olympus IX81 inverted microscope, equipped with wide-field epifluorescence illumination, was used to carry out the experiments, using 10 \times (UPlanFL N, numerical aperture (NA) 0.30), 20 \times (UPlanSApo, NA 0.75), and 60 \times PlanApoN, NA 1.45) objectives (Olympus). Fluorescence images were recorded using a Zyla 4.2 PLUS CMOS camera (Andor Technology) and a micromanager software (version 1.4.14). Images were processed and analyzed in FIJI (ImageJ) and MATLAB (Mathworks) using self-written scripts.

For the liposomes settled in the collection chamber, z-stacks were taken in three different fluorescent channels (GUV membrane: Rh-PE, GUV lumen: AF647-dextran, SUV membrane: PE-CF) with a suitable step-size. Using ImageJ, z-projections were obtained for each channel: maximum projection for the GUV membrane to obtain the equatorial plane of the GUVs, and average projection for the GUV lumen as well as SUV membrane. The average projection of the SUV membrane was used to normalize the illumination profile of the other two projections. Using a MATLAB Script, the average projection of the liposomal lumens was smoothed to get one unique local maximum per liposome. Liposomes too close to the edges of the image were ignored. The detected local maxima were used as centers on the corresponding GUV membrane channel to obtain radial intensity profiles as a function of angle. The distance from the center to the maxima in each radial profile was measured as the radius for that angle. Finally, the median of these radii was taken as the radius of the liposome.

For the GUVs being produced and flowing downstream in the postjunction channel, images were obtained in the GUV membrane channel (Rh-PE). Using ImageJ, individual liposomes were cropped and concatenated into a stack. If required, StackReg plugin was used to align the centers of the individual liposomes. A band-pass filter was used to appropriately filter out large as well as small structures. The obtained stack was then processed further using a similar MATLAB script as described above. Unlike the previous method, however, the centers of the GUVs were obtained using either the QI tracker^[71] or by tracking the circular arcs of the liposome membrane and mapping the center. A similar analysis was performed on the time-lapse data obtained for liposomes immobilized in microfluidic traps. The liposomes whose diameter was greater than the channel height was further corrected as explained in Note 1 in the Supporting Information. In order to obtain the histograms for the Eu^{3+} -SDIP assay, background intensity was first subtracted from the intensity of the liposome lumen.

Supporting Information

Supporting Information is available from the Wiley Online Library or from the author.

Acknowledgements

The authors would like to thank Jacob Kerssemakers for help with the MATLAB code. This work was supported by the NWO TOP-PUNT grant (no. 718014001), the Netherlands Organisation for Scientific Research (NWO/OCW) as part of the NanoFront and BaSyC programs, and European Research Council Advanced Grant SynDiv (No. 669598). S.D. and C.D. conceived the experiments. S.D., S.W., and D.H. performed the experiments. S.D. and S.W. analyzed the data. S.D., S.W., and C.D. wrote the paper.

Conflict of Interest

The authors declare no conflict of interest.

Keywords

growth, hybrid vesicles, liposomes, membrane fusion, membrane tension, microfluidics, synthetic cells

Received: June 3, 2019

Revised: July 18, 2019

Published online: July 31, 2019

- [1] A. C. Forster, G. M. Church, *Mol. Syst. Biol.* **2006**, 2, 45.
- [2] J. W. Szostak, D. P. Bartel, P. L. Luisi, *Nature* **2001**, 409, 387.
- [3] N. A. Yewdall, A. F. Mason, J. C. M. van Hest, *Interface Focus* **2018**, 8, 20180023.
- [4] K. Göpflich, I. Platzman, J. P. Spatz, *Trends Biotechnol.* **2018**, 36, 938.
- [5] T. Trantidou, M. Friddin, Y. Elani, N. J. Brooks, R. V. Law, J. M. Seddon, O. Ces, *ACS Nano* **2017**, 11, 6549.
- [6] V. Noireaux, A. Libchaber, *Proc. Natl. Acad. Sci. USA* **2004**, 101, 17669.
- [7] P. M. Gardner, K. Winzer, B. G. Davis, *Nat. Chem.* **2009**, 1, 377.
- [8] C. Xu, S. Hu, X. Chen, *Mater. Today* **2016**, 19, 516.
- [9] P. Van Nies, I. Westerlaken, D. Blanken, M. Salas, M. Mencía, C. Danelon, *Nat. Commun.* **2018**, 9, 1583.
- [10] Y. Mulla, A. Aufderhorst-Roberts, G. H. Koenderink, *Phys. Biol.* **2018**, 15, 041001.
- [11] I. Ivanov, R. B. Lira, T.-Y. D. Tang, T. Franzmann, A. Klosin, L. C. da Silva, A. Hyman, K. Landfester, R. Lipowsky, K. Sundmacher, R. Dimova, *Adv. Biosyst.* **2019**, 3, 1800314.
- [12] J. B. Parsons, C. O. Rock, *Prog. Lipid Res.* **2013**, 52, 249.
- [13] S. W. White, J. Zheng, Y.-M. Zhang, C. O. Rock, *Annu. Rev. Biochem.* **2005**, 74, 791.
- [14] G. Van Meer, D. R. Voelker, G. W. Feigenson, *Nat. Rev. Mol. Cell Biol.* **2008**, 9, 112.
- [15] J. C. M. Holthuis, A. K. Menon, *Nature* **2014**, 510, 48.
- [16] Y. A. Chizmadzhev, *Biochem. (Moscow) Suppl. Ser. A: Membr. Cell Biol.* **2012**, 6, 152.
- [17] L. V. Chernomordik, M. M. Kozlov, *Nat. Struct. Mol. Biol.* **2008**, 15, 675.
- [18] R. Jahn, T. Lang, T. C. Südhof, *Cell* **2003**, 112, 519.
- [19] M. M. Kozlov, L. V. Chernomordik, *Curr. Opin. Struct. Biol.* **2015**, 33, 61.
- [20] T. T. Kliesch, J. Dietz, L. Turco, P. Halder, E. Polo, M. Tarantola, R. Jahn, A. Janshoff, *Sci. Rep.* **2017**, 7, 1.
- [21] F. S. Cohen, M. H. Akabas, A. Finkelstein, *Science* **1982**, 217, 458.
- [22] A. Finkelstein, J. Zimmerberg, F. S. Cohen, *Annu. Rev. Physiol.* **1986**, 48, 163.
- [23] L. V. Chernomordik, G. B. Melikyan, Y. A. Chizmadzhev, *Biochim. Biophys. Acta, Rev. Biomembr.* **1987**, 906, 309.
- [24] J. Zimmerberg, F. S. Cohen, A. Finkelstein, *Science* **1980**, 210, 906.
- [25] J. C. Shillcock, R. Lipowsky, *Nat. Mater.* **2005**, 4, 225.
- [26] V. Knecht, S. J. Marrink, *Biophys. J.* **2007**, 92, 4254.
- [27] W. K. Spoelstra, S. Deshpande, C. Dekker, *Curr. Opin. Biotechnol.* **2018**, 51, 47.
- [28] L. Jin, N. P. Kamat, S. Jena, J. W. Szostak, *Small* **2018**, 14, 1.
- [29] I. A. Chen, J. W. Szostak, *Biophys. J.* **2004**, 87, 988.
- [30] M. M. Hanczyc, S. M. Fujikawa, J. W. Szostak, *Science* **2003**, 302, 618.
- [31] I. Budin, J. W. Szostak, *Proc. Natl. Acad. Sci. USA* **2011**, 108, 5249.
- [32] G. Murtas, *Syst. Synth. Biol.* **2010**, 4, 85.
- [33] J. Dervaux, V. Noireaux, A. J. Libchaber, *Eur. Phys. J. Plus* **2017**, 132, 1.
- [34] R. Wick, P. L. Luisi, *Chem. Biol.* **1996**, 3, 277.
- [35] P. K. Schmidli, P. Schurtenberger, P. L. Luisi, *J. Am. Chem. Soc.* **1991**, 113, 8127.
- [36] M. Exterkate, A. Caforio, M. C. A. Stuart, A. J. M. Driessen, *ACS Synth. Biol.* **2018**, 7, 153.
- [37] A. Bhattacharya, R. J. Brea, H. Niederholtmeyer, N. K. Devaraj, *Nat. Commun.* **2019**, 10, 1.
- [38] A. Scott, M. J. Noga, P. de Graaf, I. Westerlaken, E. Yildirim, C. Danelon, *PLoS One* **2016**, 11, e0163058.
- [39] K. Kurihara, M. Tamura, K. Shohda, T. Toyota, K. Suzuki, T. Sugawara, *Nat. Chem.* **2011**, 3, 775.
- [40] K. Takakura, T. Toyota, T. Sugawara, *J. Am. Chem. Soc.* **2003**, 125, 8134.
- [41] M. D. Hardy, J. Yang, J. Selimkhanov, C. M. Cole, L. S. Tsimring, N. K. Devaraj, *Proc. Natl. Acad. Sci. USA* **2015**, 112, 8187.
- [42] P.-A. Monnard, D. W. Deamer, *Anat. Rec.* **2002**, 268, 196.
- [43] S. Deshpande, Y. Caspi, A. E. C. Meijering, C. Dekker, *Nat. Commun.* **2016**, 7, 10447.
- [44] S. Deshpande, W. K. Spoelstra, M. Van Doorn, J. Kerssemakers, C. Dekker, *ACS Nano* **2018**, 12, 2560.
- [45] S. Deshpande, A. Birnie, C. Dekker, *Biomicrofluidics* **2017**, 11, 034106.
- [46] S. Deshpande, C. Dekker, *Nat. Protoc.* **2018**, 13, 856.
- [47] D. Needham, R. S. Nunn, *Biophys. J.* **1990**, 58, 997.
- [48] M. M. Koslov, V. S. Markin, *J. Theor. Biol.* **1984**, 109, 17.
- [49] K. Olbrich, W. Rawicz, D. Needham, E. Evans, *Biophys. J.* **2000**, 79, 321.
- [50] F. R. Hallett, J. Marsh, B. G. Nickel, J. M. Wood, *Biophys. J.* **1993**, 64, 435.
- [51] K. Ogłęcka, P. Rangamani, B. Liedberg, R. S. Kraut, A. N. Parikh, *eLife* **2014**, 3, e03695.
- [52] L. V. Chernomordik, M. M. Kozlov, G. B. Melikyan, I. G. Abidor, V. S. Markin, Y. A. Chizmadzhev, *Biochim. Biophys. Acta, Biomembr.* **1985**, 812, 643.
- [53] J. Akagi, K. Khoshmanesh, B. Evans, C. J. Hall, K. E. Crosier, J. M. Cooper, P. S. Crosier, D. Wlodkowic, *PLoS One* **2012**, 7, e36630.
- [54] M. Chabanon, J. C. S. Ho, B. Liedberg, A. N. Parikh, P. Rangamani, *Biophys. J.* **2017**, 112, 1682.
- [55] B. R. Lentz, *Eur. Biophys. J.* **2007**, 36, 315.
- [56] C. Y. Cheng, J. Y. Wang, R. Kausik, K. Y. C. Lee, S. Han, *Biomacromolecules* **2012**, 13, 2624.
- [57] B. R. Lentz, J. K. Lee, *Mol. Membr. Biol.* **1999**, 16, 279.
- [58] J. Yang, M. H. Shen, *Methods Mol. Biol.* **2006**, 325, 59.
- [59] T. Tanaka, M. Yamazaki, *Langmuir* **2004**, 20, 5160.
- [60] Y.-H. M. Chan, B. van Lengerich, S. G. Boxer, *Biointerphases* **2008**, 3, FA17.
- [61] D. P. Pantazatos, R. C. MacDonald, *J. Membr. Biol.* **1999**, 170, 27.
- [62] R. B. Lira, T. Robinson, R. Dimova, K. A. Riske, *Biophys. J.* **2019**, 116, 79.
- [63] T. Robinson, P. E. Verboket, K. Eyer, P. S. Dittrich, *Lab Chip* **2014**, 14, 2852.
- [64] L. Gao, R. Lipowsky, J. Shillcock, *Soft Matter* **2008**, 4, 1208.
- [65] S. Deshpande, F. Brandenburg, A. Lau, M. G. F. Last, K. W. Spoelstra, L. Reese, S. Wunna, M. Dogterom, C. Dekker, *Nat. Commun.* **2019**, 10, 1800.
- [66] T. F. Zhu, I. Budin, J. W. Szostak, *Methods Enzymol.* **2013**, 533, 275.
- [67] J. B. Segur, H. E. Oderstar, *Ind. Eng. Chem.* **1951**, 43, 2117.
- [68] V. S. Malinin, P. Frederik, B. R. Lentz, *Biophys. J.* **2002**, 82, 2090.
- [69] P. L. Hansen, J. A. Cohen, R. Podgornik, V. A. Parsegian, *Biophys. J.* **2003**, 84, 350.
- [70] N. P. Money, *Plant Physiol.* **1989**, 91, 766.
- [71] M. T. J. Van Loenhout, J. W. J. Kerssemakers, I. De Vlaminck, C. Dekker, *Biophys. J.* **2012**, 102, 2362.